Journal of the European Ceramic Society 16 (1996) 3-14

0955-2219/96/$15.00
0955-2219(95)00175-1

Model Experiments Concerning Abnormal Grain Growth in Silicon Nitride

Wolfgang Dressler,[a*] Hans-Joachim Kleebe,[b†] Michael J. Hoffmann,[a] Manfred Rühle[b] & Günter Petzow[a]

[a]Max-Planck-Institut für Metallforschung, Institut für Werkstoffwissenschaft, Pulvermetallurgisches Laboratorium, Heisenbergstr. 5, D-70569 Stuttgart 80, Germany
[b]Max-Planck-Institut für Metallforschung, Institut für Werkstoffwissenschaft, Seestraße 92, D-70174 Stuttgart 1, Germany

(Received 30 December 1994; accepted 9 September 1995)

Abstract

Model experiments were designed to study abnormal grain growth in Si_3N_4-based ceramics. Experiments relating inhomogeneous crystalline secondary-phase distribution to exaggerated grain growth conclusively showed that abnormal grain growth is not governed by secondary-phase distribution, because a rapid homogenization of locally formed liquid occurs via capillary forces. Further investigations were focussed on intrinsic properties of the α-Si_3N_4-starting powders. The influence of: (i) β-Si_3N_4-grain morphology; (ii) β-Si_3N_4-nuclei density, and (iii) β-Si_3N_4-grain-size distribution of the powder blends on microstructural development were analyzed. The results revealed that a large basal plane of β-Si_3N_4 seeds energetically and kinetically favours grain growth. However, this effect is only partly responsible for abnormal grain growth. The formation of elongated Si_3N_4 grains, such as in in situ *reinforced Si_3N_4 materials, strongly depends on the amount and grain-size distribution of β-Si_3N_4 nuclei present in the α-Si_3N_4-starting powder.*

1 Introduction

Silicon nitride-based ceramics exhibit excellent mechanical and thermo-mechanical properties. However, potential engineering application is strongly limited owing to their given brittleness, i.e. their low fracture toughness.[1,2] A number of research activities focussed on the study of possible toughening mechanisms in ceramic materials.[3-14] Investigations on the reinforcement of monolithic ceramic matrices by incorporation of discontinuous secondary phases, such as metallic particles, SiC whiskers or platelets, have provided some basic understanding of the complex crack/microstructure interaction.[15,16] The observed increase in fracture resistance was mainly attributed to crack deflection and crack bridging mechanisms.[1,2,17,18] In some cases crack branching was also observed.[19] However, reinforcing ceramic matrices with secondary phases may also limit the applicability of such composites, in particular, because the achieved toughness improvement can be limited: (i) to relatively low service temperatures; (ii) by an anisotropic toughness within the composite or (iii) difficulties during densification. Therefore, one of the most promising toughening strategy is the reinforcement by elongated Si_3N_4 grains, grown *in situ* in a fine-grained Si_3N_4 matrix.[20-22] This would result in a highly isotropic toughness up to high service temperatures and no restricted densification, provided that densification to closed porosity (about 94% theoretical density) can be completed before exaggerated *in situ* growth of β-Si_3N_4 grains takes place. A number of studies were reported on the observation of abnormal grain growth in Si_3N_4 ceramics prepared with various metal-oxide additions and densified by different processing techniques.[23-25] In these investigations a correlation between resulting fracture toughness and the morphology of β-Si_3N_4 grains was found. In particular, a higher aspect ratio as well as a higher grain diameter yields an improved fracture resistance.[26,27] It was recently reported that the same toughening effect applies for liquid-phase sintered SiC ceramics with *in situ* grown large α-SiC particles embedded in a fine grained matrix.[28-30] It should be noted that the strength of *in situ* toughened, completely densified Si_3N_4 ceramics can be limited by the occurence of large

*Now at Technische Hochschule Darmstadt, Fachbereich Materialwissenschaft, Fachgebiet Disperse Feststoffe, Hilpertstraße, 31/D, D-64295 Darmstadt, Germany.
†Now at Universität Bayreuth, Lehrstuhl für Keramik und Verbundwerkstoffe, Ludwig Thoma Straße 36 B, D-95440 Bayreuth, Germany.

β-Si_3N_4 grains, since they may act as crack initiation sites.[25]

The observation of exaggerated grain growth and its relation to improved fracture resistance in Si_3N_4 ceramics is well established. However, only limited studies are reported on the effect of intrinsic β-Si_3N_4-grain characteristics on microstructural variations upon densification.[22-27] No model experiments, verifying possible parameters affecting exaggerated grain growth, have been reported to date. Therefore, this paper is based on model experiments designed to study abnormal grain growth in Si_3N_4 ceramics. Apart from a model proposed for the inhomogeneous distribution of crystalline secondary phases enhancing grain growth, the intrinsic properties of the Si_3N_4-starting powders were investigated. In this context, the influence of the β-Si_3N_4-grain morphology, the β-Si_3N_4-nuclei density, and the β-Si_3N_4 grain-size distribution within the starting powder blends on exaggerated grain growth are discussed.

2 Experimental Procedures

2.1 Inhomogeneous distribution of crystalline secondary phases

Post-sintered reaction bonded Si_3N_4 material (SRBSN), containing approximately 20–25 vol% of elongated β-Si_3N_4 particles in the microstructure, was processed. The Si-powder blend, containing 5 wt% Y_2O_3 + 1 wt% Al_2O_3(Y/Al) as sintering aids, was dry milled in a planetary mill. The Si-powder compacts were prepared by uniaxial die-pressing and subsequent cold isostatic pressing at 630 MPa. All powder compacts were nitrided subject to a heating-rate of 6°C/h, a maximum temperature of 1420°C, a nitridation atmosphere of 90 vol% N_2 and 10 vol% H_2, a gas pressure of 950 mbars and a nitriding time of 120 h. Post-densification involved a two-step gas-pressure sintering cycle: 1875°C, 90 min at 0·5 MPa N_2 and 1920°C, 60 min at 10 MPa N_2. The microstructure evolution and, in particular, the formation of crystalline secondary phases were studied by X-ray diffraction at early stages of nitridation. In addition, nitrided samples as well as materials processed by deliberately interrupting the sintering cycle at intermediate temperatures of 1550, 1650, 1750, and 1850°C were studied by SEM and TEM. Secondary phase identification was performed by both X-ray diffraction and electron diffraction (during TEM observations). Microstructure characterization of the materials prepared by model experiments, described below, was performed using optical microscopy.

2.1.1 Model experiment using an embedded, pre-synthesized crystalline phase

Additive doped (24·1 wt% Yb_2O_3 + 0·5 wt% Al_2O_3) silicon nitride powder compacts (UBE-SN-E10, further designated as E10; β = 4·1%) with embedded crystalline Ca-stabilized Yb–apatite-($Yb_9Ca(SiO_4)_6ON$) as well as Yb–silicate-phases ($Yb_2Si_2O_7$) were produced by cold isostatic pressing at 630 MPa. Yb–apatite- and Yb–silicate-powders were received by precipitation of $Yb(OH)_3$ onto SiO_2 (formation of Yb–silicate) or SiO_2 and Si_3N_4 (formation of Yb–apatite) from an alkaline (pH = 11) 0·5 molar $Yb(NO_3)_3$ solution and subsequent calcination at 800°C according to Gröbner.[31] The crystallization of the cold isostatically pressed (55 MPa) powder compacts was performed at 1600°C, 1 h at 0·1 MPa N_2 (Yb–apatite) and 1400°C, 14 h in air ($Yb_2Si_2O_7$). The model specimens, consisting of a Si_3N_4 powder compact which contained a crystalline secondary-phase core, were subjected to a heat treatment at 1700°C for a period of 1 h under 0·1 MPa N_2.

2.1.2 Model experiment preparing a sandwich specimen

A sintered (1780°C, 50 min, 0·1 MPa N_2 + 10 min, 1·6 MPa N_2) additive containing (10·7 wt% Y_2O_3 + 3·6 wt% Al_2O_3) Si_3N_4 specimen was cut into three plates (SN1, SN2, SN3). $Y_2Si_2O_7$-powder was produced by ultrasonic mixing of Y_2O_3 and SiO_2 in n-hexan for 5 min. After cold isostatic pressing (630 MPa) the powder compacts were crystallized in air using a heating time of 14 h and a maximum temperature of 1400°C. The crystalline $Y_2Si_2O_7$-silicate (YS) was arranged between two dense Si_3N_4 slabs (SN1, SN2) of the pre-sintered material. This sandwich specimen and, as a reference, the third Si_3N_4-plate (SN3) were heat treated for 1 h at 1800°C under a nitrogen pressure of 0·1 MPa.

2.2 Influence of β-Si_3N_4 particle morphology

An α-rich Si_3N_4 powder (UBE-SN-ESP, further designated as ESP; α > 97%), attrition milled with 11·5 wt% Y_2O_3 + 2·9 wt% Al_2O_3 used as sintering aids, was subsequently doped with 5 vol% β-Si_3N_4 whiskers (UBE-SN-WB) and mixed in a roller mill, in order to avoid extensive whisker damage during processing. Powder compacts were prepared via cold-isostatic pressing at 630 MPa. After densification of these powder blends via gas-pressure sintering (1930°C, 1 h at 10 MPa N_2) polished and plasma-etched specimen surfaces were investigated by SEM.

2.3 Effect of initial β-Si_3N_4 nuclei density and grain-size distribution

Two α-rich Si_3N_4 powders (E10 and ESP) doped with various amounts of equiaxed β-Si_3N_4 nuclei

Table 1. Powder characteristics of the Si_3N_4-starting powders and powder blends. The β-Si_3N_4 content and β-crystallite radius of the powder mixtures are calculated using the rule of mixture

Powder	β-*content* (*vol %*)	β-*crystallite-radius* (μ*m*)	*Denka powder content* (*vol %*)	*Nuclei density* (*N*/μ*m*^{3})
UBE-SN-ESP (ESP)	3	0·10	0	6·5
UBE-SN-E10 (E10)	4·1	0·06	0	40·8
Denka	97·5	0·14	0	76·3
Denka/ESP 4/96	6·8	0·10	4	9·3
Denka/ESP 8/92	10·6	0·10	8	12·1
Denka/E10 4/96	7·8	0·06	4	42·2
Denka/E10 20/80	22·8	0·08	20	48

(see Table 1), using a Denka starting powder with a β-Si_3N_4 content of approximately 97%, were applied to study the influence of initial β-Si_3N_4 content on the final microstructure by comparing the microstructural development of the doped and undoped powders. The β-Si_3N_4 content, as well as the crystallite size of the starting powders and mixtures, were determined by means of X-ray analysis applying a Seyffert powder diffractometer and the Scherrer equation, which correlates the peak broadening (β) with the crystallite radius (r). The instrumental peak broadening (I = 0·1429°) was determined by measuring the peak width of the 111-peak of a stress free silicon single crystal. This results in the following equation:

$$r = \frac{1}{2} \cdot \frac{0{\cdot}89 \cdot \lambda}{(\beta - \mathrm{I}) \cdot \cos \Theta} \quad (1)$$

where λ is the wave length of the X-ray radiation (λ = 154·056 pm) and θ is the peak position. The evaluation was performed by using the (210) α-Si_3N_4 reflection. Detailed sedimentation experiments of the used starting powders and X-ray analysis of the generated grain-size fractions, which were discussed in detail elsewhere,[25] revealed that the grain-size distributions of the α- and β-particles are similar. This enables the determination of the β-Si_3N_4-crystallite size by measuring the average size of the α-crystals. Then the nuclei density, N, of the starting powders and mixtures can be calculated from:[25]

$$N = \frac{3}{4 \cdot 10^4 \cdot \pi} \cdot \sum_i \frac{\beta_i \cdot A_i}{r^3_{\beta i}} \quad (2)$$

In this equation β_i is the volume fraction of β-Si_3N_4, A_i the Si_3N_4-content (vol%) and $r_{\beta i}$ the β-crystallite size of the participating starting powders. The powder characteristics are summarized in Table 1. Densification was achieved by adding 10 vol% sintering aids (Y_2O_3 + Al_2O_3) either by gas pressure sintering (1950°C, 1 h at 10 MPa N_2) or by pressureless sintering (1780°C, 20 min at 0·1 MPa N_2) in a graphite resistance furnace.

2.4 Microstructural characterization

The overall microstructure of the materials was investigated by optical microscopy, scanning electron microscopy (SEM), and transmission electron microscopy (TEM). SEM investigations were performed using polished and subsequently plasma-etched surfaces of the consolidated materials. TEM foils were prepared following standard techniques, which involve grinding, dimpling, and ion thinning to electron transparency. The TEM foils were finally coated with a light carbon film to reduce charging under the electron beam.

Quantitative microstructural evaluation was performed using a semi-automatic image analyser of Imtronic (Computer-Vertriebs-Union, Berlin). This PC operated apparatus enables not only the automatic and interactive reconstruction of the grain boundary network but also the measurement of the minimum and maximum Ferret-diameter of each reconstructed grain. This analysis provides the 2-dimensional length/aspect-ratio distribution of the observed microstructure. In order to get sufficient statistical reliability at least 2000 grains of the quantitative analysed microstructures were measured. Owing to the fact that the known toughening models are based on the real 3-dimensional particle parameters, the 3-dimensional length/aspect-ratio distribution was calculated by means of a novel computer program (for further details see Refs 25 and 32).

3 Results

3.1 Inhomogenous distribution of crystalline secondary phases

Low magnification SEM and TEM studies of the Y/Al-doped material after nitridation, but before final densification, revealed crystalline secondary phases in the RBSN. Additional X-ray diffraction analysis parallel to electron diffraction studies on these phases indicated the formation of H-phase, $Y_5(SiO_4)_3N$, at an early stage of nitridation (see Fig. 1). After consolidation, the material exhibited

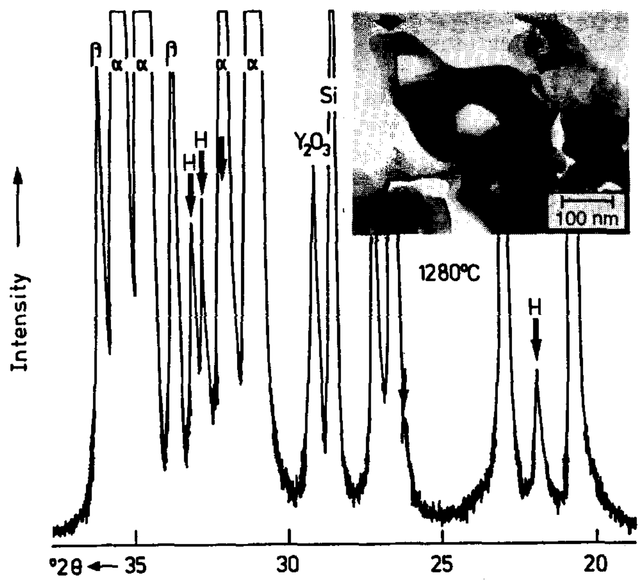

Fig. 1. X-ray diffraction pattern of the Y/Al-doped RBSN material revealing the H-phase formation at an early stage of nitridation (nitriding temperature = 1280°C). The inset shows a TEM bright-field image of the H-phase in the nitrided sample (RBSN).

an overall microstructure consisting of about 20–25% by volume of large elongated β-Si_3N_4 grains embedded in a fine-grained matrix, as depicted in Fig. 2. Crystalline secondary phases were present at triple-grain junctions. During SEM observations of Y/Al-fluxed materials, obtained by interrupting the gas-pressure sintering cycle at temperatures of 1550, 1650, and 1750°C, only homogeneous, fine-grained silicon nitride particles were evident. However, the onset of the formation of elongated silicon nitride grains was observed at higher sintering temperatures ≥1850°C. This result is consistent with findings from Mitomo *et al.*,[27] who reported the onset of abnormal grain growth at about 1850°C. The experimental results regarding the microstructural development, based on SEM and TEM observations, suggest a growth mechanism schematically depicted in Fig. 3.

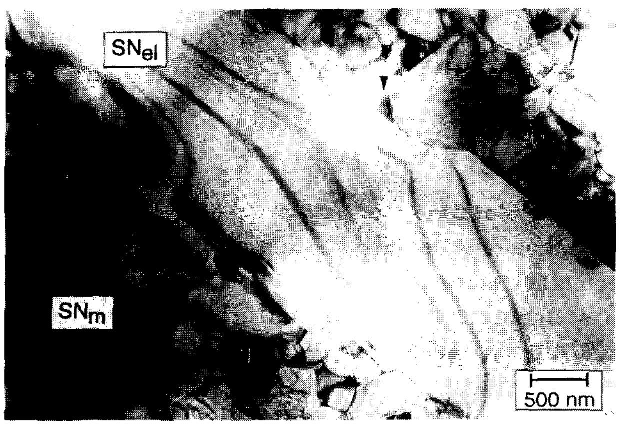

Fig. 2. Low magnification TEM bright-field image of Y/Al-containing SRBSN showing elongated β-Si_3N_4 grains (SN_{el}) in a fine-grained β-Si_3N_4 matrix (SN_m). The darker regions in the image correspond to the crystalline secondary phase located at multi-grain junctions.

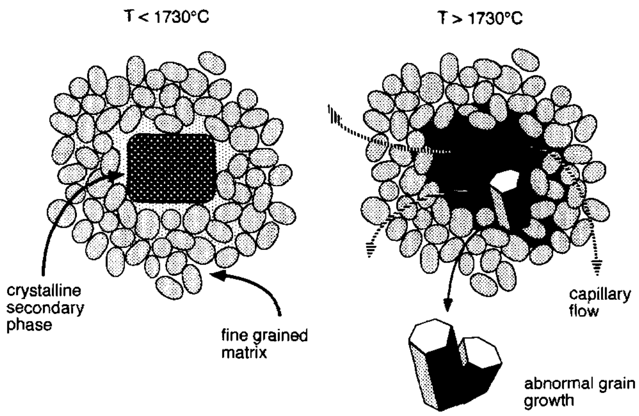

Fig. 3. Schematic illustration of the proposed mechanism of the elongated-grain formation for an inhomogeneous distribution of crystalline secondary phases.

In the proposed model it is assumed that metastable crystalline secondary phases, revealing a high thermal stability field,[33,34] are already formed at an early stage of densification. The assumption is supported by the X-ray diffraction findings at temperatures as low as 1280°C (see also Fig. 1). During subsequent sintering, these phases remain stable up to their melting point, while the eutectic liquid has already formed at a lower temperature and facilitates initial densification. The eutectic temperature in the SiO_2–Si_3N_4–Y_2O_3 ternary system lies at 1550°C (filled triangle in the phase diagram shown in Fig. 4).[35,36] The eutectic temperature, however, is lower owing to the Al_2O_3-content of the Si-starting powder blend. With increasing temperature, dissolution/reprecipitation occurs simultaneously with the α/β-Si_3N_4-phase transformation, which is complete at about 1650°C for these materials. At 1630°C (cross-section of the phase diagram in Fig. 4), the secondary H-phase is still crystalline. Even at 1730°C (dashed line in the diagram), this phase still lies

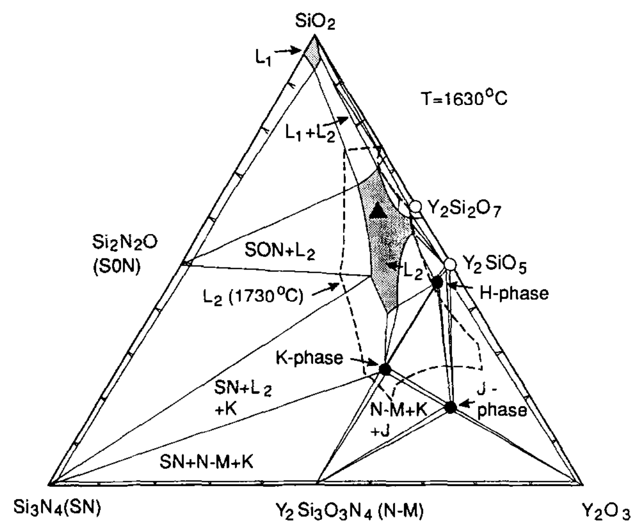

Fig. 4. Phase diagram for the Y_2O_3–Si_3N_4–SiO_2 system indicating the H-phase.[35,36]

outside the liquid phase field. It is thought that the crystalline secondary phase only melts at higher sintering temperatures, forming excess liquid. This excess liquid is inhomogeneously distributed over the entire sample, owing to the inhomogeneous distribution of crystalline secondary phase at lower sintering temperatures, which is thought to initiate both increased densification and the onset of abnormal grain growth. A strong increase in densification rate at temperatures of about 1800°C was experimentally confirmed by dilatometer measurements during sintering. Moreover, the formation of large, elongated β-Si_3N_4 grains, randomly oriented in the sintered body, was also reported.[36] It is thought that some of the excess liquid will progress through the RBSN pore channels by capillary forces and simultaneously permit densification, but it is presumed in this model that excess liquid remains at the site containing the original metastable Y–Si–oxinitride phase. This liquid would act as a flux for the rapid growth of highly-elongated β-Si_3N_4 grains by a dissolution–reprecipitation process.

The proposed model is based on two requirements. Firstly, upon liquid formation the wetting liquid should not be drawn completely out of the central reservoir into the surrounding porous RBSN matrix. This situation could arise if the volume of liquid exceeds the porosity in the RBSN and also, if densification occurs simultaneously with capillary extrusion. Secondly, exaggerated β-Si_3N_4 grain growth and elongation is required to occur at the liquid reservoir, whereas normal coarsening should prevail in the surrounding matrix. To prove these requirements additional model experiments were designed.

3.1.1 Model experiment using an embedded pre-synthesized crystalline phase

In order to verify the model described above a large piece of pre-synthesized crystalline secondary phase (5 mm in diameter) was embedded in a Si_3N_4-powder compact and subsequently consolidated, as schematically depicted in Fig. 5. It was expected that in the region around the embedded crystalline secondary phase, or at the secondary phase/matrix interface, a high amount of excess liquid was formed during sintering, which would strongly enhance abnormal grain growth. However, optical and scanning electron microscopy on cross-sections of the samples revealed an unexpected result, as shown in Fig. 6. In the case of the Yb–silicate ($Yb_2Si_2O_7$) containing material, a large pore, containing a small pocket of residue secondary phase, had formed at the site of the formerly embedded pre-synthesized crystalline secondary phase (Fig. 6 (a)). This seemingly suggests that the excess liquid was nearly completely drawn from the central reservoir into the bulk material upon sintering. A closer inspection of the boundary between the residue secondary phase and the Si_3N_4-bulk (compare Fig. 6 (b)) gave no evidence for enhanced exaggerated grain growth in this region. The apatite ($Yb_9Ca(SiO_4)_6ON$) containing material revealed a similar behaviour. The secondary phase was completely drawn into the bulk and no abnormal grain growth was observed. Hence, it is concluded that, in the present model

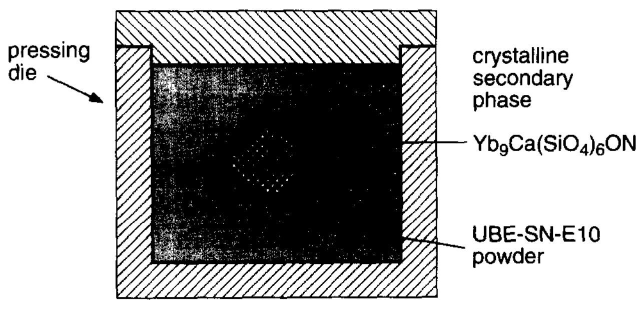

Fig. 5. Schematic illustrating the cold-isostatic pressing arrangement of silicon nitride green bodies with an embedded crystalline secondary phase.

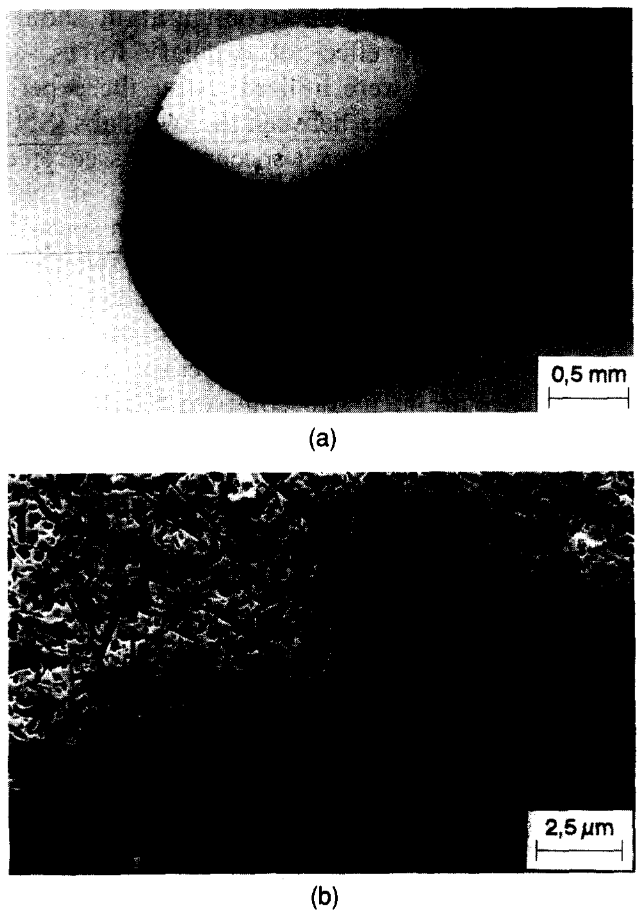

Fig. 6. Secondary phase containing specimen (compare Fig. 5) after heat treatment (1700°C, 1 h, 0·1 MPa N_2). (a) Optical micrograph showing the residue secondary phase pocket (white), the Si_3N_4 bulk material (gray), the formed hole (black), and a thin film of embedding material (dark gray). (b) SEM micrograph of the boundary between the secondary phase and the bulk material showing no abnormal grain growth.

experiments, high capillary forces were responsible for an homogeneous distribution of the excess liquid phase throughout the samples, which resulted in microstructures indistinguishable from materials sintered without the incorporation of crystalline phases. The main difference between the inhomogeneities (excess liquid) formed during post-sintering of reaction-bonded Si_3N_4 (see section 3.1) and the liquid generated in the present model specimens is that at the beginning of the sintering process the deliberately created inhomogeneities are surrounded by a highly porous Si_3N_4-powder compact. Therefore, a second model experiment was designed to minimize the porosity effect.

3.1.2 Model experiment preparing a sandwich specimen

In order to suppress the influence of high capillary forces, a sandwich specimen was prepared using a dense Si_3N_4 slab with the pre-synthesized crystalline secondary phase and another dense Si_3N_4 slab on top, as schematically shown in Fig. 7. This sandwich and the reference (SN3) were heated above the melting temperature of the crystalline secondary phase and a cross section of the joined sample was prepared. This configuration should greatly reduce the effect of capillary forces, as dense Si_3N_4 slabs were utilized. After the experiment, the contact area between the two slabs (SN1 and SN2) of the sandwich specimen was covered with a secondary phase film. Hence, it was thought that enhanced abnormal grain growth would occur at the interface between the two slabs and the interlayer. SEM microscopy studies of the cross sections, however, revealed that the microstructural development of the model specimen and the reference are identical (compare Fig. 8 (a and b)). No pronounced exaggerated grain growth was observed.

Diffusion processes along the interface led to a uniform distribution of the secondary phase between the two Si_3N_4-slaps at the applied sintering temperatures, where all secondary phase present in the system is thought to be liquid. The reported results clearly exclude the initially proposed effect of inhomogeneously distributed crystalline secondary phases on abnormal grain growth in Si_3N_4

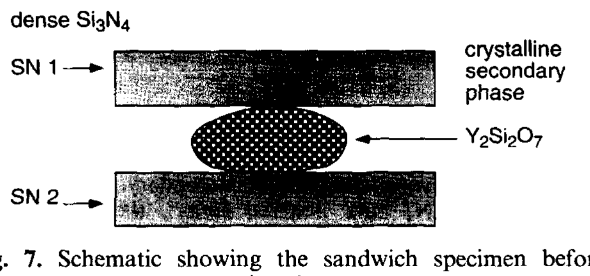

Fig. 7. Schematic showing the sandwich specimen before sintering.

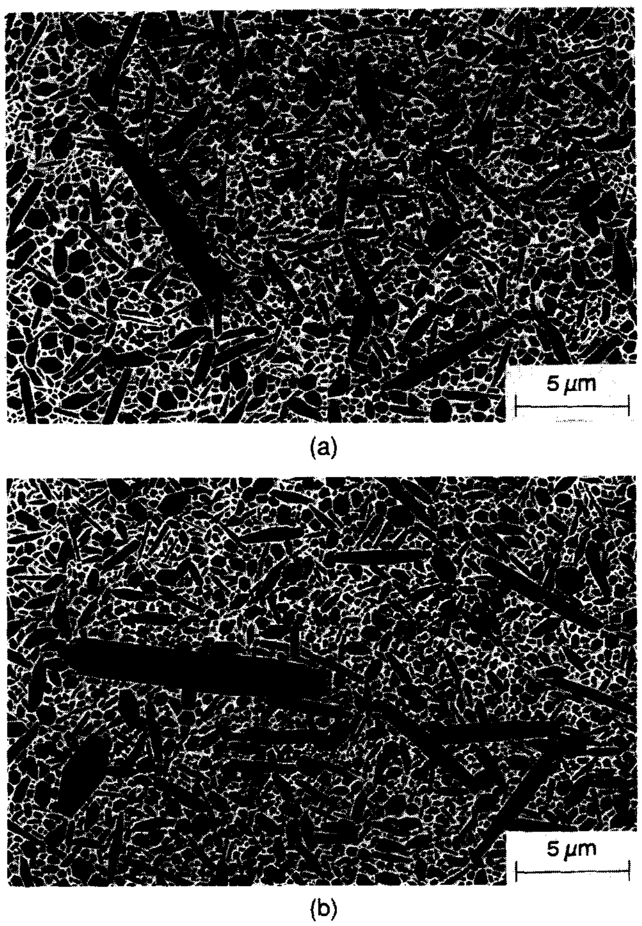

Fig. 8. Microstructures of (a) the sandwich specimen (directly at the edge where the material was in contact with the secondary phase) and (b) reference specimen after a heat treatment at 1800°C for a period of 1 h under 0·1 MPa N_2. The SEM micrographs show no significant difference in grain-size distribution. This suggests that an inhomogeneous distributed liquid phase does not cause abnormal grain growth.

materials. Accordingly, the development of exceptionally large grains has to be due to intrinsic powder properties such as the α/β-Si_3N_4-content and grain-size distribution as well as the β-nuclei morphology, which is discussed in the following sections.

3.2 Influence of β-Si_3N_4 particle morphology

The influence of the intrinsic morphology of β-Si_3N_4 particles present in the starting powder on the microstructural development of gas-pressure sintered materials was studied. An α-rich Si_3N_4 powder was therefore doped with 5 vol% β-Si_3N_4 whiskers. After densification of the powder blend, the microstructure of the consolidated material was investigated by optical microscopy and SEM on polished and plasma-etched specimen surfaces. Plasma etching is a very sensitive technique regarding small chemical changes in the material. The etching rate strongly depends on the Al-content of the Si_3N_4 grains; a higher Al-concentration in the solid solution results in a lower plasma-etching rate.

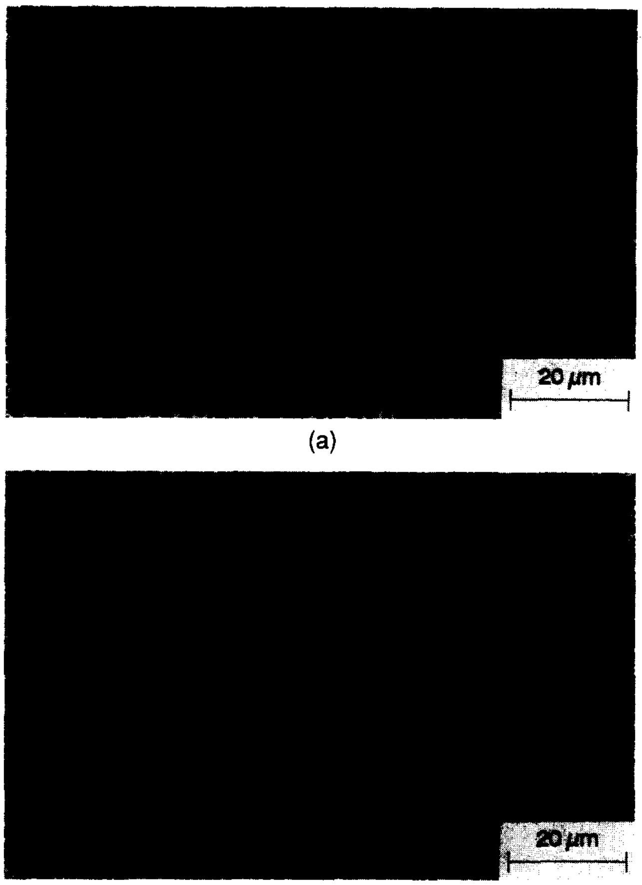

Fig. 9. Influence of powder morphology on microstructural development. Microstructures of (a) β-Si_3N_4 whisker doped and (b) undoped UBE-SN-ESP materials after gas pressure sintering (1930°C, 60 min, 10 MPa N_2).

Figure 9 shows the microstructures of the β-Si_3N_4 whisker doped (a) and the undoped (b) ceramics. The β-Si_3N_4 whisker containing material possesses a significantly greater number of large elongated grains, which have a deeper etched core surrounded by a rim structure. Analytical TEM-measurements reveal that the core is Al free while the rim structure contains, apart from Si and N, additional Al and O (Fig. 10 (a and b)). These findings and the fact that the observed cores are elongated and aligned parallel to the length direction of the abnormally grown crystals (Fig. 11) suggest that the Al-containing outer region of the large elongated β-Si_3N_4 grains grew epitaxially on the starting Al-free β-Si_3N_4 whiskers. Owing to the kinetic growth advantage of the basal plane compared to the prism planes in Si_3N_4 crystals,[37,38] the whiskers revealed a higher growth rate in length direction rather than in width upon sintering. The aspect ratio of the epitaxially grown region (excluding the core) of the large β-crystal shown in Fig. 11 (a) amounts to about 23. In contrast to this, the aspect ratio of the initial β-Si_3N_4 nuclei runs to about 4·5. In comparison to the more globular, equiaxed β-Si_3N_4 grains present in the

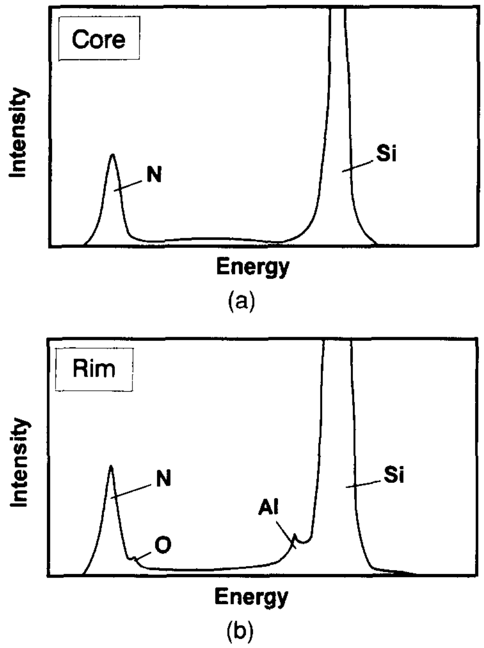

Fig. 10. EDX-analysis (TEM) of an elongated large β-Si_3N_4-crystal in the β-Si_3N_4 whisker doped material consisting of (a) an Al-free core and (b) an Al-containing rim structure (see also Fig. 11(b)).

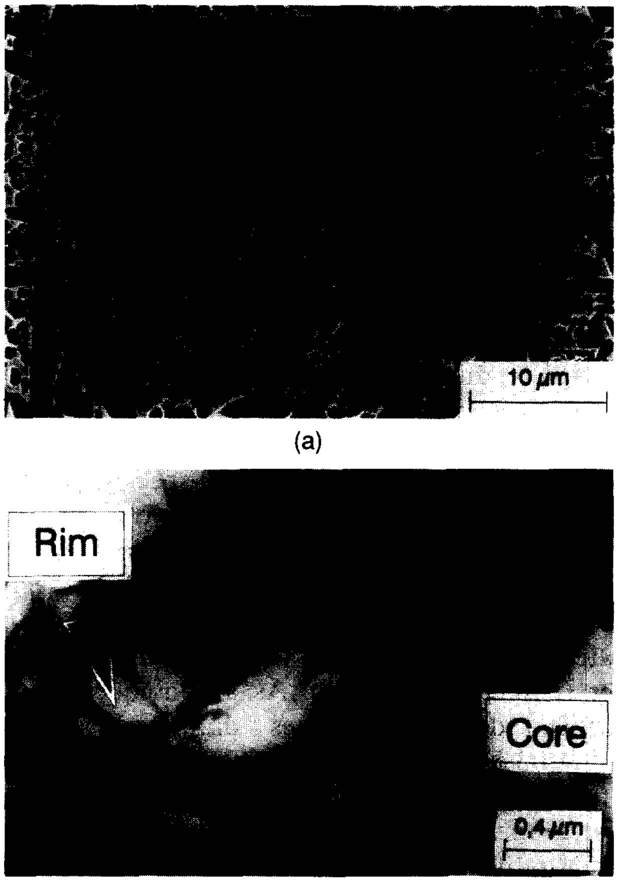

Fig. 11. (a) SEM-micrograph of a large β-Si_3N_4-grain possessing a deeper etched core (Al-free) having an aspect ratio of 4·5 and a rim structure with an aspect ratio of 23. (b) TEM-micrograph of a β-Si_3N_4-crystal with an elongated core-structure.

starting powder, the added whiskers showed, right from the beginning of sintering, a relatively high growth rate of the basal planes and, hence, exhibited very large grains (> 50 μm) with high aspect ratios (up to 15). It is important to note that the initially elongated shape of the whiskers remains during the α–β-transformation and the following grain coarsening. The results seemingly suggest that it is possible to directly influence the resulting microstructure via the morphology of the pre-existing β-Si_3N_4 nuclei, as the morphology of whisker-like particles is preserved during consolidation.

3.3 Effect of initial β-Si_3N_4 nuclei density and β-Si_3N_4 grain-size distribution

Two α-rich Si_3N_4 powders (E10 and ESP), doped with various amounts of equiaxed β-Si_3N_4 nuclei, using a Denka starting powder with a β-Si_3N_4 content of approximately 97%, were utilized to study the influence of initial β-Si_3N_4 content on the final microstructure.

In the case of α-rich ESP powders the β-Si_3N_4 doping results in a grain refinement, because the number of grains per unit area raises from 0·56 N/μm^2 for the undoped specimen to 0·72 N/μm^2 and 0·86 N/μm^2 by increasing the amount of β-nuclei from 6·5 N/μm^3 (undoped) to 9·3 N/μm^3 and 12·1 N/μm^3 in the starting powder, as can be seen from Table 1 and Fig. 12. It is important to note that the average crystallite size of the α-(ESP: r = 0·10 μm) and the added β-powder (Denka: r = 0·14 μm) are in the same order of magnitude. This result is consistent with investigations reported by Iskoe *et al.*,[39] who assumed that the dissolution of β-Si_3N_4 during densification is negligible.

In contrast to the results of the ESP material (grain refinement), SEM analysis of polished and plasma-etched surfaces of the E10-specimens show a coarsening of the general microstructure with increasing β-Si_3N_4-nuclei density, as can be seen from Fig. 13. Here, the added β-Si_3N_4-nuclei (Denka) are about two times larger in size compared to the β-particles in the α-rich starting powder (E10: r = 0·06 μm). As a consequence, the particle density decreases dramatically from 30·5 to 3·5 N/μm^3 by increasing the β-nuclei density from 40·8 to 76·3 N/μm^3. The size-shape histograms (weighted by volume) derived from quantitative microstructural analysis of Denka/E10-specimens reveal a decrease of the volume fraction of grains having a length smaller than 0·5 μm from 11·5 vol% (E10) to 0·5 vol% (Denka) with increasing β-Si_3N_4-content (see Fig. 14). Simultaneously, the mean grain length and grain diameter increases from 0·36 to 0·80 μm and from 0·12 to 0·45 μm, respectively. Additionally, low β-doping leads to an enhanced grain growth in the length direction, but to a decrease in aspect ratio of the coarser grains (Denka/E10 4/96), owing to the initially large grain width of the added β-particles (Denka). Further addition of β-nuclei (Denka/E10 20/80) results in a reduction of the maximum grain length and aspect ratio. Utilizing pure β-Si_3N_4 (Denka) powder as starting material produces a homogeneous equiaxed microstructure possessing a low mean aspect ratio of 1·8 in comparison to specimens sintered from α-rich-powder (E10) which exhibited a mean aspect ratio of 2·7.

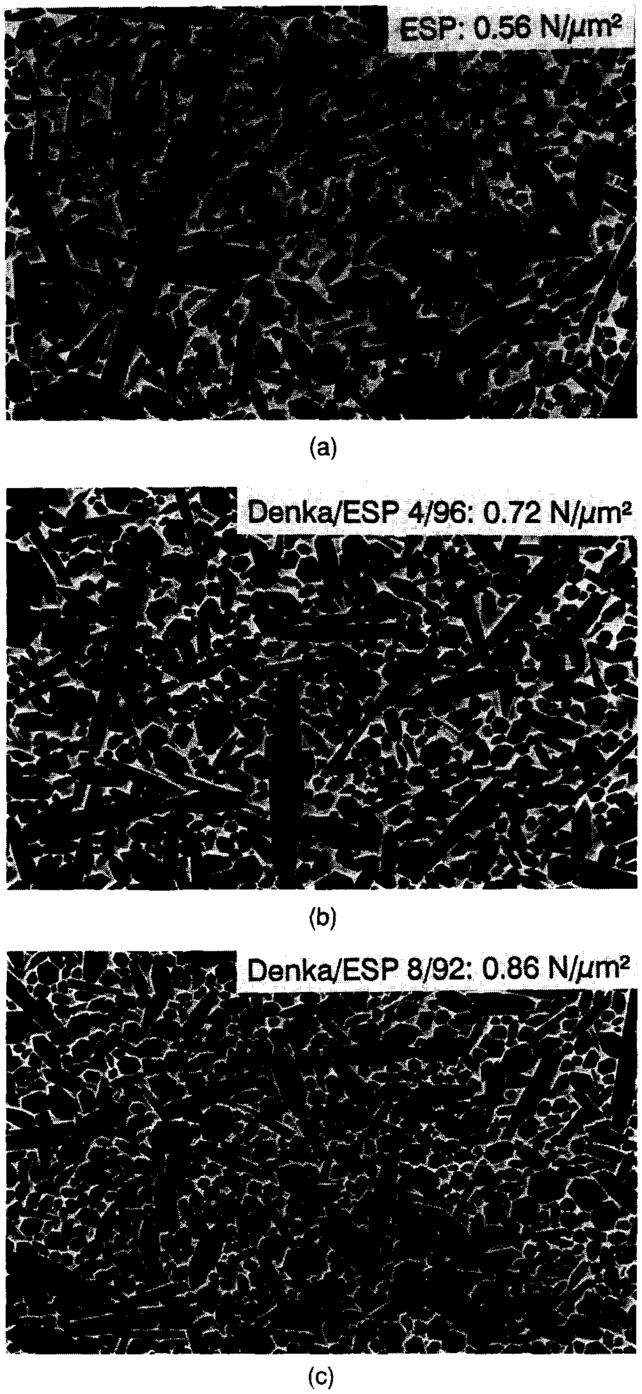

Fig. 12. Microstructure of gas pressure sintered (1950°C, 1 h, 10 MPa N_2) (a) undoped ESP; (b) Denka/ESP-mixture 4/96, and (c) Denka/ESP-mixture 8/92. The number of grains per unit area rises from (a) 0·56 N/μm^2 and (b) 0·72 N/μm^2 to (c) 0·86 N/μm^2 by increasing the amount of β-nuclei from (a) 6·5 N/μm^3 and (b) 9·3 N/μm^3 to (c) 12·1 N/μm^3 in the starting powder.

4 Discussion

4.1 Secondary phase inhomogeneities

The experimental results clearly showed that the formation of crystalline secondary phases at an early stage of sintering does not govern abnormal grain growth. It is concluded that high capillary forces draw the excess liquid into the bulk of the material, resulting in a higher densification rate and, as a consequence, in a uniform microstructure. No enhanced exaggerated grain growth was observed in either of the model experiments performed. Most importantly, the specimen containing a residue pocket of secondary phase after sintering (see Fig. 6) reveals no abnormal grain growth into the remaining glass pocket. The obtained microstructures after densification, utilizing pre-synthesized crystalline phases, were indistinguishable from the microstructures observed after sintering of common starting powder compacts.

4.2 Intrinsic powder properties

Since the generated secondary phase inhomogeneities do not cause the often observed abnormal grain growth, the intrinsic powder properties must be responsible for the exaggerated growth of individual crystals. The β-Si_3N_4 doping of α-rich powders on the one hand results in grain refinement if the dopant (Denka) possesses a comparable crystallite size to the α-rich matrix powder (ESP) and if the nuclei density is low (see Table 1 and Fig. 12). On the other hand, provided that the added β-nuclei (Denka) are larger than the β-particles in the α-rich powder (E10) and that the nuclei density is high, grain coarsening is observed (see Table 1 and Figs 13, 14), since the β-Si_3N_4/β-Si_3N_4 particle interaction is enhanced.

The results presented clearly revealed that, if the β-Si_3N_4 nuclei density reaches a certain value, depending on the grain-size distribution of the starting powder, a dissolution of the smaller β-Si_3N_4 particles is observed followed by a coarsening of the microstructure. These results can be explained using the model schematically shown in Fig. 15. In this diagram C_G^{α} and C_G^{β} represent the equilibrium concentrations of α- and β-particles in a

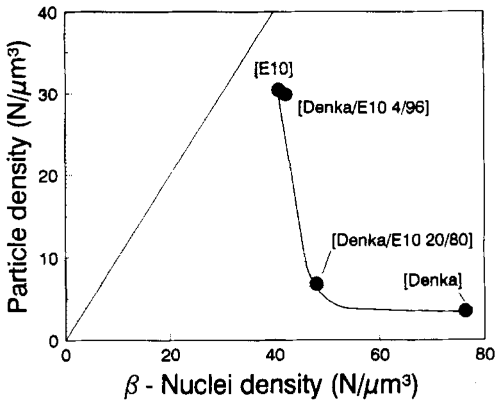

Fig. 13. Influence of β-nuclei density in the starting powder on particle density of sintered Si_3N_4-ceramics. Within the dotted area the particle density is higher than the nuclei density. Since the investigated specimens are located outside the dotted area it is suggested that no nucleation takes place during sintering.

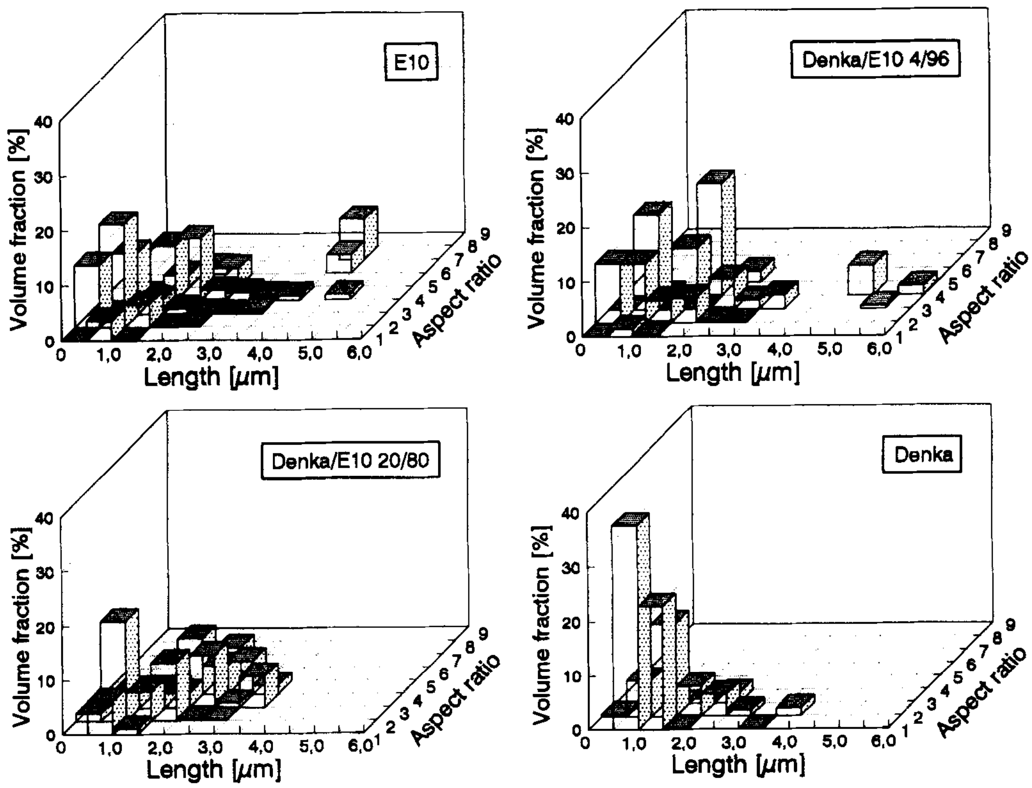

Fig. 14. Quantitative microstructural analysis of Denka/E10-composites with various ratios of mixture. (a) 0/100, (b) 4/96, (c) 20/80, and (d) 100/0.

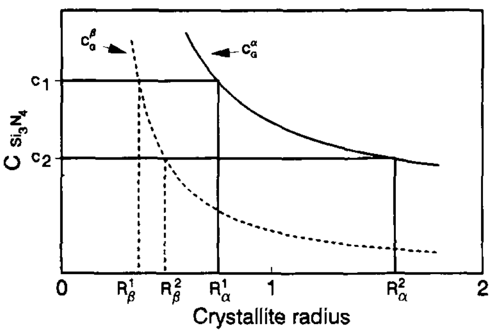

Fig. 15. Dependency of equilibrium concentrations of α- and β-Si_3N_4 modification on crystallite radius. If the Si_3N_4-concentration in the liquid decreases from C_1 to C_2 the critical radii of dissolution increase from R_β^1 to R_β^2 and from R_α^1 to R_α^2.

solvent. According to Wagner[40] these concentrations depend on the radius of the crystal (R), the surface energy σ, the temperature T as well as the constants C_0 and K, as summarized in the following equation:

$$C_G = C_0 \cdot \exp\left(\frac{\sigma}{R} \cdot \frac{K}{T}\right) \tag{3}$$

This relation has been derived by assuming a spherical shape of the examined particles. A deviation of the spherical morphology results in a different constant K, as calculated by Dressler.[25] Since the transformation enthalpy of the reaction α-Si_3N_4 $\rightarrow$ β-Si_3N_4 is negative, the equilibrium concentration of the α-phase, C_G^α, must be higher in comparison to C_G^β, as depicted in Fig. 15. C_1 and C_2 are arbitrary Si_3N_4-concentrations in the liquid phase directly at the particle surface during the solution reprecipitation process, which causes the α/β- transformation as well as the grain coarsening. In the Ostwald Ripening model of Wagner[40] these concentrations depend on the particle dimension and the mean concentration of the solute, because the crystals in this model are isolated from each other and thus the concentration gradients do not overlap. In contrast to that, the solid phase fraction in our experiments is so high that the Si_3N_4 concentrations at the particle surfaces are controlled by the surrounding crystals and their size distribution. At a given Si_3N_4-concentration in the liquid (C_1 or C_2) the radii $R_\beta^{1,2}$ and $R_\alpha^{1,2}$ are critical grain sizes, which means that all particles being smaller dissolve whereas larger crystals grow.

This model predicts the dissolution of small β-crystals if they are located within the diffusion gradient of a larger β-particle. For example: a small β-particle having a crystallite radius between R_β^1 and R_β^2 dissolute if the Si_3N_4-concentration in the liquid phase directly at its surface is reduced from c_1 to c_2 due to the growth of an adjacent larger β-crystal. This condition is satisfied in the case of the Denka/E10-specimens (see Figs 13 and 14). By adding the coarse β-rich Denka powder to the fine grained E10 the small β-nuclei of the E10-powder start to dissolve in an early stage of α/β-transformation owing to the increase of the critical radius of dissolution (R_β). In the case of the Denka/ESP-materials, the β-Si_3N_4-nuclei density is lower and the added β-particles are of the same sizes. Thus, the probability that two β-crystals influence each other is lower and, due to the smaller size difference, the Denka β-grains cannot dissolve the ESP β-nuclei. Consequently, the particle density after sintering increases by raising the amount of β-particles in the starting powder, as depicted in Fig. 12, which leads to a grain refinement.

The increase in maximum particle length observed at low β-doping of E10-powder (see Fig. 14) as well as the globularization and the simultaneous decrease of the maximum grain length by further raising the β-Si_3N_4-fraction can also be explained by this model. At low concentrations of coarse β-Si_3N_4-particles (Denka/E10 4/96, see Table 1) these grains grow by dissolution of the surrounding α- and β-Si_3N_4-crystals. If the amount of large β-grains is further increased (Denka/E10 20/80, see Table 1) growth in the length direction of the coarse particles is reduced due to steric hindrance. The effect of steric hindrance was shown by growth experiments performed by Krämer and Hoffmann.[41,42] Moreover, large particles consume more material during grain growth in comparison to smaller crystals, which also causes a reduction in aspect ratio.

In Fig. 16 the abnormal grain growth of the whisker doped material (see also Fig. 11) is shown schematically. The exceptionally high growth rate in the c-direction is due to the large basal plane of the β-Si_3N_4-whiskers. This large basal plane corresponds to a very low equilibrium concentration of

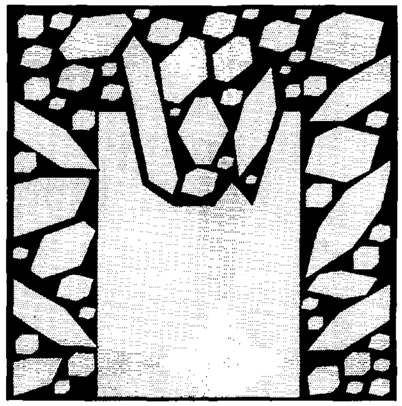

Fig. 16. Model of abnormal grain growth in Si_3N_4-ceramics. The larger particles reduce the Si_3N_4-concentration in front of their basal plane and thus dissolute smaller particles in growth direction. This enables abnormal grain growth of crystals possessing a large basal plane in comparison to the surrounding particles.

Si_3N_4 in the surrounding liquid phase (see Fig. 15). Therefore, close to the abnormal growing particles the critical radius of dissolution is extraordinarily high. This enables the very fast dissolution of adjacent smaller particles and the observed exceptionally high aspect ratio (23) of the rim structure grown during sintering.

The investigations unequivocally reveal that a broad β-Si_3N_4-grain-size distribution in the starting powder causes exaggerated grain growth due to solution of α- as well as small β-Si_3N_4-particles and reprecipitation onto larger β-Si_3N_4-grains. Moreover, the morphology of the initially existing β-crystals also influences the resulting microstructure of the sintered ceramic. In addition, the effect of abnormal grain growth is enhanced by high sintering temperatures and long sintering times, as shown in earlier investigations.[25]

5 Summary

Inhomogeneous distribution of crystalline secondary phases, formed at an early stage of consolidation, can lead to a local enrichment of the liquid phase during sintering at elevated temperatures. However, based on model experiments it can be concluded that crystalline secondary phases do not govern exaggerated grain growth, since a rapid homogenization of locally formed liquid occurs via capillary forces. A large basal plane of growing β-particles surrounded by smaller β-crystals or dissolving α-Si_3N_4 grains enhances grain growth due to kinetic and energetic reasons. Model experiments clearly showed that the formation of such elongated particles, grown *in situ* in the Si_3N_4 matrices, strongly depends on the amount, grain-size distribution, and morphology of β-Si_3N_4 nuclei in the starting powder.

6 Conclusions

Earlier studies confirm that an appreciable toughening effect can be monitored in Si_3N_4-based ceramics owing to the *in situ* development of elongated β-Si_3N_4 grains. However, in order to reach high fracture toughness accompanied by high strength, the abnormal grain growth has to be controlled. By using α-Si_3N_4-starting powders having a broad intrinsic β-Si_3N_4 grain-size distribution unfavourably large particles may grow, which can act as crack initiation sites. In order to optimize mechanical properties, Si_3N_4-powders should possess a narrow β-Si_3N_4-grain-size distribution and have faceted, elongated β-Si_3N_4-crystals. Ceramics prepared from such starting powders should exhibit microstructures containing a large amount of elongated Si_3N_4-grains without exaggerated grain growth development, and therefore combine both high strength and high fracture toughness.

The results presented show that tailoring of the final Si_3N_4 microstructures becomes possible by controlling the β-Si_3N_4-nuclei in the starting powder.

Acknowledgement

The authors are greatly indepted to Elmar Hampp for preparing the crystalline phases used in the model experiments and for helpful discussions.

References

1. Evans, A. G, Perspective on the development of high-toughness ceramics. *J. Am. Ceram. Soc.*, **73**(2) (1990) 187–206.
2. Becher, P. F., Microstructural design of toughened ceramics. *J. Am. Ceram. Soc.*, **74**(2) (1991) 255–69.
3. Lange, F. F., Fracture toughness of Si_3N_4 as a function of the initial α-content. *J. Am. Ceram. Soc.*, **62**(7–8) (1979) 428–30.
4. Faber, K. T. & Evans, A. G., Crack deflection processes — I. Theory. *Acta Metall.*, **31**(4) (1983) 565–76.
5. Becher, P. F. & Wei, G. C., Toughening behaviour in SiC-whisker-reinforced alumina. *J. Am. Ceram. Soc.*, **67**(12) (1984) C267–9.
6. Evans, A. G. & McMeeking, R. M., On the toughening of ceramics by strong reinforcements. *Acta Metall.*, **34**(12) (1986) 2435–41.
7. Rühle, M., Dalgleish, B. J. & Evans, A. G., On the toughening of ceramics by whiskers. *Scr. Metall.*, **21**(5) (1987) 681–6.
8. Becher, P. F., Hsueh, C.-H., Angelini, P. & Tiegs, T. N., Toughening behavior in whisker-reinforced ceramic matrix composites. *J. Am. Ceram. Soc.*, **71**(12) (1988) 1050–61.
9. Campbell, G. H., Rühle, M., Dalgleish, B. J. & Evans, A. G., Whisker toughening: a comparison between aluminium oxide and silicon nitride toughened with silicon carbide. *J. Am. Ceram. Soc.*, **73**(3) (1990) 521–30.
10. Kleebe, H.-J., Corbin, N. D., Willkens, C., & Rühle, M., Transmission electron microscopy studies of silicon nitride/silicon carbide interfaces. *Mat. Res. Soc. Symp. Proc.*, **170** (1990) 79–84.
11. Bengisu, T. M., Inal, O. T. & Tosyali, O., On whisker toughening in ceramic materials. *Acta Metall. Mater.*, **39**(11) (1991) 2509–17.
12. Mitomo, M. & Uenosono, S., Gas-pressure sintering of β-silicon nitride. *J. Mater. Sci.*, **26** (1991) 3940–4.
13. Kawashima, T., Okamoto, H., Yamamoto, H. & Kitamura, A., Grain size dependence of the fracture toughness of silicon nitride ceramics. *J. Ceram. Soc. Jpn.*, **99**(4) (1991) 320–3.
14. Hirao, K., Nagaoka, T., Brito, M. E. & Kanzaki, S., Microstructure control of silicon nitride by seeding with rodlike β-silicon nitride particles. *J. Am. Ceram. Soc.*, **77**(7) (1994) 1857–62.
15. Rödel, J., Crack closure forces in ceramics; characterization and formation. *J. Eur. Ceram. Soc.*, **9** (1992) 323–34.
16. Lawn, B., *Fracture of brittle solids*, Second Edition. Cambridge University Press, Cambridge, UK, 1993.
17. Rödel, J., Interaction between crack deflection and crack bridging. *J. Eur. Ceram. Soc.*, **10** (1992) 143–50.

18. Steinbrech, R. W., Toughening mechanisms for ceramic materials. *J. Eur. Ceram. Soc.*, **10** (1992) 131–42.
19. Kleebe, H.-J., Unger, S., Meißner, E. & Ziegler, G., Microstructure and toughness correlation in silicon nitride ceramics. In *Proc. of 8th CIMTEC*, Florenz, Italy, 28 June–4 July (1994), in press.
20. Tani, E., Umebayashi, S., Kishi, K., Kobayashi, K. & Nishijima, M., Gas-pressure sintering of Si_3N_4 with concurrent addition of Al_2O_3 and 5 wt% rare earth oxide: High fracture toughness Si_3N_4 with fiber-like structure. *Am. Ceram. Soc. Bull.*, **65**(9) (1986) 1311–15.
21. Hwang, C. J. & Tien, T.-Y., Microstructural development in silicon nitride ceramics. *Materials Science Forum*, **47** (1989) 84–109.
22. Wu, F., Zhuang, H., Ma, L. & Fu, X., Self-reinforced silicon nitride by gas-pressure sintering. *Ceram. Eng. Sci. Proc.*, **14**(1–2) (1993) 321–32.
23. Hirosaki, N., Akimune, Y. & Mitomo, M., Effect of grain growth of β-silicon nitride on strength, Weibull modulus, and fracture toughness. *J. Am. Ceram. Soc.*, **76**(7) (1993) 1892–4.
24. Hampp, E., Konstitution, Sinterverhalten und Eigenschaften von Keramiken auf der Basis des Systems Si_3N_4–Yb_2O_3–SiO_2. Ph. D. Thesis, University of Stuttgart (1993).
25. Dressler, W., Gefügeentwicklung und mechanische Eigenschaften von Si_3N_4-Keramiken. Ph.D. Thesis, University of Stuttgart (1993).
26. Mitomo, M., Tsutsumi, M., Tanaka, H., Uenosono, S. & Saito, F., Grain growth during gas-pressure sintering of β-silicon nitride. *J. Am. Ceram. Soc.*, **73**(8) (1990) 2441–5.
27. Mitomo, M. & Uenosono, S., Microstructural development during gas-pressure sintering of α-silicon nitride. *J. Am. Ceram. Soc.*, **75**(1) (1992) 103–8.
28. Padture, N. P. & Lawn, B., Short-crack properties of *in situ* silicon carbide with heterogeneous microstructure. *J. Am. Ceram. Soc.*, (1994), in press.
29. Padture, N. P., *In situ* toughened silicon carbide. *J. Am. Ceram. Soc.*, **77**(2) (1994) 519–23.
30. Lee, S. K. & Kim. C. H., Effects of α-SiC versus β-SiC starting powders on microstructure and fracture toughness of SiC sintered with Al_2O_3–Y_2O_3 additives. *J. Am. Ceram. Soc.*, **77**(6) (1994) 1655–8.
31. Gröbner, J., Synthese und Charakterisierung von Yb–silikaten und Yb–Oxinitriden. Thesis, University of Stuttgart (1991).
32. Hartmann, S., Mücklich, F., Ohser, H. J., Dressler, W. & Petzow, G., Quantitative Charakterisierung von Si_3N_4-Gefügen durch räumliche Parameter. *Proceedings Metallographietagung*, Dresden 1992; Sonderbände der Praktischen Metallographie, **24** Riederer Verlag, 1993.
33. Wills, R. R., Stewart, R. W., Cunningham, J. A. & Wimmer, J. M., The silicon lanthanide oxynitrides. *J. Mater. Sci.*, **11** (1976) 749–59.
34. Wills, R. R., Holmquist, S., Wimmer, J. M. & Cunningham, J. A., Phase relationships in the system silicon nitride–yttria–silica. *J. Mater. Sci.*, **11** (1976) 1305–9.
35. Braue, W., Wötting, G. & Ziegler, G., Influence of sintering conditions and mechanical properties at room and high temperatures for selected Y–Al–Si–O–N materials. *Science of Ceramics*, **13** (1986) 341–5.
36. Kleebe, H.-J. & Ziegler, G., Influence of crystalline secondary phases on the densification behavior of RBSN during post-sintering under increased nitrogen pressure. *J. Am. Ceram. Soc.*, **72**(12) (1989) 2314–17.
37. Krämer, M., Untersuchungen zur Wachstumskinetik von β-Si_3N_4 in Keramiken und Oxinitridgläsern. Ph.D. Thesis, University of Stuttgart (1991).
38. Lai, K.-R. & Tien, T.-Y., Kinetics of β-Si_3N_4 grain growth in Si_3N_4 ceramics sintered under nitrogen pressure. *J. Am. Ceram. Soc.*, **76**(1) (1993) 91–6.
39. Iskoe, J. L. & Lange, F. F., Development of microstructure and mechanical properties during hot pressing of Si_3N_4. *Ceramic Microstructures '76, With Emphasis on Energy Related Applications*, 1976, pp. 669–78.
40. Wagner, C., Theorie der Alterung von Niederschlägen durch Umlösen. *Zeitschrift für Elektrochemie*, **65** (1961) 581–91.
41. Krämer, M., Hoffmann, M. J. & Petzow, G., Grain growth kinetics of Si_3N_4 during α/β transformation. *Acta Metall. Mater.*, **41**(10) (1993) 2939–47.
42. Hoffmann, M. J., Analysis of microstructural development and mechanical properties of Si_3N_4 ceramics. In *Tailoring Mechanical Properties of Si_3N_4 Ceramics*, eds M. J. Hoffmann & G. Petzow, Cluwer Academic Publ, Dortrecht, NATO ASI Series I: Applied Science, **246** 1994 pp. 59–72.